# Numerical simulation and computational modeling of thermo-electro-magnetic stress in anisotropic plates using scientific computing algorithms

Nazokat Sayidova*[a], Behzod Tahirov[a], Fazilat Norova[a], Humoyun Sultonov[a]
[a]Bukhara State University, 11, M. Iqbol Street, Bukhara, Uzbekistan

## ABSTRACT

This study presents a computational approach to analyze the nonlinear thermo-electro-magnetic stress behavior in anisotropic plates with complex geometries. The model is formulated based on the Hamilton-Ostrogradsky variational principle and the Kirchhoff-Love hypothesis, and solved numerically using Finite Element Method. The simulation incorporates coupled nonlinear partial differential equations representing mechanical displacements, heat conduction, and electromagnetic field interactions. Computational experiments are implemented using Python-based scientific computing tools, enabling efficient solution of the high-complexity system. Results show that electromagnetic effects increase structural deflection by approximately 11%, while combined thermal effects lead to a 16% increase. The study demonstrates the value of numerical modeling and algorithmic implementation in simulating multiphysics interactions in advanced materials, contributing to improved predictive analysis in structural informatics.

**Keywords:** computational modeling, anisotropic plates, thermo-electro-magnetic effects, finite element method, Hamilton-Ostrogradsky, scientific computing, structural informatics, variational principles

## 1. INTRODUCTION

The integration of multiphysical field interactions — namely thermal, electrical, and magnetic effects — into structural analysis has driven significant advancements in computational modeling. With the emergence of high-performance computing and open-source scientific libraries, researchers have developed robust algorithms for simulating nonlinear behavior in complex anisotropic materials.

Foundational frameworks such as the Finite Element Method and its modern implementations via software like FEniCS and COMSOL Multiphysics have enabled efficient simulation of coupled partial differential equations. These tools simplify solving nonlinear variational formulations derived from principles like Hamilton-Ostrogradsky, especially in thin-plate geometries governed by the Kirchhoff-Love hypothesis.

Recent studies focus on automating multiphysics simulations using Python, enhancing reproducibility and reducing computation time. Others emphasize material-specific simulation, such as in functionally graded materials under electromagnetic heating or thermoelastic analysis in smart composites.

Moreover, AI and machine learning approaches are being adopted to predict and optimize structural responses, bridging informatics and material modeling disciplines. Research into hybrid solvers and mesh refinement strategies also contributes to numerical stability and accuracy in large-scale simulations.

Together, these works establish a comprehensive foundation for the computational modeling of anisotropic plates influenced by thermo-electro-magnetic effects, serving as a springboard for further development in informatics-driven structural optimization.

*tahirovbehzod5@gmail.com

Fourth International Conference on Digital Technologies, Optics, and Materials Science (DTIEE 2025),
edited by Khamza Eshankulov, Arthur Gibadullin, Proc. of SPIE Vol. 13662,
136620E · © 2025 SPIE · 0277-786X · doi: 10.1117/12.3072192

## 2. PROBLEM STATEMENT

In the present study, the nonlinear thermo-electro-magnetic behavior of anisotropic plates with complex geometries is modeled using the Hamilton-Ostrogradsky variational principle and the Kirchhoff-Love hypothesis. These formulations lead to a strongly coupled system of nonlinear partial differential equations, incorporating heat conduction, electromagnetic interactions, and mechanical displacement fields.

From a computational perspective, the governing equations are discretized using the Finite Element Method, enabling numerical implementation in Python and COMSOL Multiphysics environments. Initial and boundary conditions are defined to simulate real-world constraints such as fixed, sliding, or mixed edge configurations. The resulting computational model serves as the basis for evaluating deflection and stress responses under varying multiphysical loading scenarios.

In the present study, the nonlinear thermo-electro-magnetic behavior of anisotropic plates with complex geometries is analyzed. The mathematical modeling is based on the Hamilton-Ostrogradsky variational principle, which is expressed as:

$$\int_t (\delta W_K - \delta W_{\Pi} + \delta W_A) dt = 0 \tag{1}$$

Where δ denotes the variation operator, $W_K$ is the kinetic energy, $W_{\Pi}$ is the potential energy, and $W_A$ represents the work done by external surface and volume forces.

To derive the equations of motion for plates of intricate shapes, the Kirchhoff-Love hypothesis is adopted, simplifying the description of displacement fields while preserving the essential physical characteristics. The thermal effects are incorporated by applying the Fourier law of heat conduction in an anisotropic and nonlinear formulation, leading to the differential equation:

$$\lambda_{i,j} T_{ij} - C_{\varepsilon} T - T \beta_{ij} \varepsilon_{ij} = 0 \tag{2}$$

Here, $j$ represents the thermal conductivity coefficients, $C_j$ characterizes the material-specific parameters, $T$ is the temperature, $T_0$ is the reference temperature, and $\varepsilon_j$ denotes the strain components.

Expanding the tensor expressions from the variational formulation, the system of nonlinear partial differential equations governing the dynamic behavior of the plate can be established as:

$$
\begin{cases}
-\rho h\frac{\partial^2 u}{\partial t^2}-hC_{1111}\frac{\partial^2 u}{\partial x^2}-\frac{h}{2}C_{1212}\frac{\partial^2 u}{\partial y^2}-\frac{h}{2}C_{1111}\frac{\partial^3 w}{\partial x^3}-\frac{h}{2}C_{1222}\frac{\partial^3 w}{\partial y^3}-\frac{h}{2}C_{1112}\frac{\partial^2 v}{\partial x^2}-\frac{h}{2}C_{1222}\frac{\partial^2 v}{\partial y^2}- \\
-(hC_{1122}+\frac{h}{2}C_{1212})\frac{\partial^2 v}{\partial x\partial y}-(\frac{h}{2}C_{1122}+\frac{h}{2}C_{1212})\frac{\partial^3 w}{\partial x\partial y^2}-(hC_{1211}+\frac{h}{2}C_{1112})\frac{\partial^2 u}{\partial x\partial y}-(\frac{h}{2}C_{1112}+\frac{h}{2}C_{1211})\frac{\partial^3 w}{\partial x^2\partial y}+ \\
+h\frac{\partial}{\partial x}(\alpha_{11}(T-T_0))+h\frac{\partial}{\partial y}(\alpha_{12}(T-T_0))+N_x+R_x+q_x+T_{zx}+\theta_{Tzx}+\theta_{\mathrm{T}}=0, \\
-\rho h\frac{\partial^2 v}{\partial t^2}-hC_{2222}\frac{\partial^2 v}{\partial y^2}-\frac{h}{4}C_{1212}\frac{\partial^2 v}{\partial x^2}-\frac{h}{2}C_{2212}\frac{\partial^2 u}{\partial y^2}-\frac{h}{2}C_{1211}\frac{\partial^2 u}{\partial x^2}-\frac{h}{2}C_{2222}\frac{\partial^3 w}{\partial y^3}-\frac{h}{4}C_{1211}\frac{\partial^3 w}{\partial x^3}- \\
-(hC_{2211}+\frac{h}{4}C_{1212})\frac{\partial^2 u}{\partial x\partial y}-(\frac{h}{2}C_{2212}+\frac{h}{2}C_{1222})\frac{\partial^2 v}{\partial x\partial y}-(\frac{h}{2}C_{2211}+\frac{h}{4}C_{1212})\frac{\partial^3 w}{\partial x^2\partial y}-(\frac{h}{2}C_{2212}+\frac{h}{4}C_{1222})\frac{\partial^3 w}{\partial x\partial y^2}+ \\
+h\frac{\partial}{\partial y}(\alpha_{22}(T-T_0))+\frac{h}{2}\frac{\partial}{\partial x}(\alpha_{12}(T-T_0))+N_y+R_y+q_y+T_{zy}+\theta_{Tzy}+\theta_{\mathrm{T}}=0, \\
-\rho h\frac{\partial^2 w}{\partial t^2}-\frac{h}{2}C_{1111}(\frac{\partial u}{\partial x}\frac{\partial^2 w}{\partial x^2}+\frac{1}{2}\frac{\partial^4 w}{\partial x^4})-\frac{h}{2}C_{1122}\frac{\partial v}{\partial y}\frac{\partial^2 w}{\partial x^2}-\frac{h}{2}\frac{\partial^4 w}{\partial x^2\partial y^2}(\frac{1}{2}C_{1122}+\frac{1}{2}C_{2211}+C_{1212})-\frac{h}{4}C_{1112}\frac{\partial u}{\partial y}\frac{\partial^2 w}{\partial x^2}- \\
-\frac{h}{2}\frac{\partial^4 w}{\partial x^3\partial y}(\frac{1}{2}C_{1112}+C_{1211})-\frac{h}{2}C_{2211}\frac{\partial u}{\partial x}\frac{\partial^2 w}{\partial y^2}-\frac{h}{2}C_{2222}(\frac{\partial v}{\partial y}\frac{\partial^2 w}{\partial y^2}+\frac{1}{2}\frac{\partial^4 w}{\partial y^4})-\frac{h}{4}C_{2212}(\frac{\partial u}{\partial y}\frac{\partial^2 w}{\partial y^2}+\frac{\partial v}{\partial x}\frac{\partial^2 w}{\partial y^2})- \\
-\frac{h}{2}\frac{\partial^4 w}{\partial x\partial y^3}(\frac{1}{2}C_{2212}+C_{1222})-hC_{1211}\frac{\partial u}{\partial x}\frac{\partial^2 w}{\partial x\partial y}-hC_{1222}\frac{\partial v}{\partial y}\frac{\partial^2 w}{\partial x\partial y}-\frac{h}{2}C_{1212}(\frac{\partial u}{\partial y}\frac{\partial^2 w}{\partial x\partial y}+\frac{\partial v}{\partial x}\frac{\partial^2 w}{\partial x\partial y})+ \\
+\frac{h}{2}\frac{\partial^2 w}{\partial x^2}\alpha_{11}(T-T_0)+\frac{h}{2}\frac{\partial^2 w}{\partial y^2}\alpha_{22}(T-T_0)+h\frac{\partial^2 w}{\partial x\partial y}\alpha_{12}(T-T_0)+\frac{h}{12}C_{1111}\frac{\partial^4 w}{\partial x^4}+\frac{h}{12}\frac{\partial^4 w}{\partial x^2\partial y^2}(C_{1122}+C_{2212}+C_{1211})+ \\
+\frac{h}{12}\frac{\partial^4 w}{\partial x^3\partial y}(C_{1112}+C_{2211})+\frac{h}{12}\frac{\partial^4 w}{\partial x\partial y^3}(C_{2222}+C_{1212})+\frac{h}{12}C_{1222}\frac{\partial^4 w}{\partial y^4}+N_z+R_z+q_z+T_{zz}+\theta_{Tzz}+\theta_{\mathrm{T}}=0, \\
\lambda_{11}\frac{\partial^2\theta_{\mathrm{T}}}{\partial x^2}+\lambda_{12}\frac{\partial^2\theta_{\mathrm{T}}}{\partial x\partial y}+\lambda_{21}\frac{\partial^2\theta_{\mathrm{T}}}{\partial y\partial x}+\lambda_{22}\frac{\partial^2\theta_{\mathrm{T}}}{\partial y^2}-C_\varepsilon\frac{\partial^2\theta_{\mathrm{T}}}{\partial t}-\theta_{\mathrm{T}_0}\beta_{11}(\frac{\partial^2 u}{\partial x\partial t}-z\frac{\partial^3 w}{\partial x^2\partial t}+\frac{1}{2}\frac{\partial^3 w}{\partial x^2\partial t})- \\
-\theta_{\mathrm{T}_0}\beta_{22}(\frac{\partial^2 v}{\partial y\partial t}-z\frac{\partial^3 w}{\partial y^2\partial t}+\frac{1}{2}\frac{\partial^3 w}{\partial y^2\partial t})-\theta_{\mathrm{T}_0}\beta_{12}(\frac{\partial^2 u}{\partial y\partial t}+\frac{\partial^2 v}{\partial x\partial t}-z\frac{\partial^3 w}{\partial x\partial y\partial t}+\frac{1}{2}\frac{\partial^3 w}{\partial x\partial y\partial t})=0.
\end{cases}
\tag{3}
$$

This system couples mechanical displacements, thermal gradients, and electromagnetic effects in a strongly nonlinear manner.

Initial conditions are specified to define the dynamic state of the plate at the starting time:

$$
\begin{aligned}
&\rho h\frac{\partial u}{\partial t}\delta u\Big|_t=0,\ \rho h\frac{\partial v}{\partial t}\delta v\Big|_t=0,\ \rho h\frac{\partial w}{\partial t}\delta w\Big|_t=0,\ \theta_T\big|_{t=0}=T_0 \\
&\rho\frac{h^3}{12}\frac{\partial^2 w}{\partial t\partial x}\delta w\Big|_{x,t}=0,\ \ \rho\frac{h^3}{12}\frac{\partial^2 w}{\partial t\partial y}\delta w\Big|_{y,t}=0
\end{aligned}
\tag{4}
$$

Where u, v, and www are the displacement components along the respective coordinate axes.

Boundary conditions are formulated based on different types of edge supports. For clamped and sliding boundary configurations, the mechanical constraints and force balances are prescribed respectively as:

$$h\left[C_{1111}\left(\frac{\partial u}{\partial x}+\frac{1}{2}\left(\frac{\partial w}{\partial x}\right)^2\right)+C_{1122}\left(\frac{\partial v}{\partial y}+\frac{1}{2}\left(\frac{\partial w}{\partial y}\right)^2\right)+C_{1112}\left(\frac{1}{2}\frac{\partial u}{\partial y}+\frac{1}{2}\frac{\partial v}{\partial x}+\frac{1}{2}\frac{\partial w}{\partial x}\frac{\partial w}{\partial y}\right)-\alpha_{11}(T-T_0)\right]\delta u\Big|_x=0,$$

$$\frac{1}{2}h\left[C_{1211}\left(\frac{\partial u}{\partial x}+\frac{1}{2}\left(\frac{\partial w}{\partial x}\right)^2\right)+C_{1222}\left(\frac{\partial v}{\partial y}+\frac{1}{2}\left(\frac{\partial w}{\partial y}\right)^2\right)+C_{1212}\left(\frac{1}{2}\frac{\partial u}{\partial y}+\frac{1}{2}\frac{\partial v}{\partial x}+\frac{1}{2}\frac{\partial w}{\partial x}\frac{\partial w}{\partial y}\right)-\alpha_{12}(T-T_0)\right]\delta v\Big|_x=0,$$

$$h\left[C_{2211}\left(\frac{\partial u}{\partial x}+\frac{1}{2}\left(\frac{\partial w}{\partial x}\right)^2\right)+C_{2222}\left(\frac{\partial v}{\partial y}+\frac{1}{2}\left(\frac{\partial w}{\partial y}\right)^2\right)+C_{2212}\left(\frac{1}{2}\frac{\partial u}{\partial y}+\frac{1}{2}\frac{\partial v}{\partial x}+\frac{1}{2}\frac{\partial w}{\partial x}\frac{\partial w}{\partial y}\right)-\alpha_{22}(T-T_0)\right]\delta v\Big|_y=0,$$

$$\frac{1}{2}h\left[C_{1211}\left(\frac{\partial u}{\partial x}+\frac{1}{2}\left(\frac{\partial w}{\partial x}\right)^2\right)+C_{1222}\left(\frac{\partial v}{\partial y}+\frac{1}{2}\left(\frac{\partial w}{\partial y}\right)^2\right)+C_{1212}\left(\frac{1}{2}\frac{\partial u}{\partial y}+\frac{1}{2}\frac{\partial v}{\partial x}+\frac{1}{2}\frac{\partial w}{\partial x}\frac{\partial w}{\partial y}\right)-\alpha_{12}(T-T_0)\right]\delta u\Big|_y=0,$$

$$\frac{h^3}{12}\left(C_{1111}\frac{\partial^2 w}{\partial x^2}+C_{1122}\frac{\partial^2 w}{\partial y^2}+C_{1112}\frac{\partial^2 w}{\partial x\partial y}\right)\delta\frac{\partial w}{\partial x}\Big|x=0,$$

$$\frac{1}{2}h\left[C_{1111}\left(\frac{\partial u}{\partial x}+\frac{1}{2}\left(\frac{\partial w}{\partial x}\right)^2\right)+C_{1122}\left(\frac{\partial v}{\partial y}+\frac{1}{2}\left(\frac{\partial w}{\partial y}\right)^2\right)+C_{1112}\left(\frac{1}{2}\frac{\partial u}{\partial y}+\frac{1}{2}\frac{\partial v}{\partial x}+\frac{1}{2}\frac{\partial w}{\partial x}\frac{\partial w}{\partial y}\right)-\alpha_{11}(T-T_0)\right]\frac{\partial w}{\partial x}\delta w\Big|x=0,$$

$$-\frac{h^3}{12}\left(C_{1211}\frac{\partial^3 w}{\partial x^2\partial y}+C_{1222}\frac{\partial^3 w}{\partial y^3}+C_{1212}\frac{\partial^3 w}{\partial x\partial y^2}\right)\delta w\Big|x=0,$$

$$\frac{1}{2}h\left[C_{1211}\left(\frac{\partial u}{\partial x}+\frac{1}{2}\left(\frac{\partial w}{\partial x}\right)^2\right)+C_{1222}\left(\frac{\partial v}{\partial y}+\frac{1}{2}\left(\frac{\partial w}{\partial y}\right)^2\right)+C_{1212}\left(\frac{1}{2}\frac{\partial u}{\partial y}+\frac{1}{2}\frac{\partial v}{\partial x}+\frac{1}{2}\frac{\partial w}{\partial x}\frac{\partial w}{\partial y}\right)-\alpha_{12}(T-T_0)\right]\frac{\partial w}{\partial y}\delta w\Big|x=0,$$

$$\frac{h^3}{12}\left(C_{2211}\frac{\partial^2 w}{\partial x^2}+C_{2222}\frac{\partial^2 w}{\partial y^2}+C_{2212}\frac{\partial^2 w}{\partial x\partial y}\right)\delta\frac{\partial w}{\partial y}\delta w\Big|y=0$$

$$\frac{1}{2}h\left[C_{2211}\left(\frac{\partial u}{\partial x}+\frac{1}{2}\left(\frac{\partial w}{\partial x}\right)^2\right)+C_{2222}\left(\frac{\partial v}{\partial y}+\frac{1}{2}\left(\frac{\partial w}{\partial y}\right)^2\right)+C_{2212}\left(\frac{1}{2}\frac{\partial u}{\partial y}+\frac{1}{2}\frac{\partial v}{\partial x}+\frac{1}{2}\frac{\partial w}{\partial x}\frac{\partial w}{\partial y}\right)-\alpha_{22}(T-T_0)\right]\frac{\partial w}{\partial y}\delta w\Big|y=0,$$

$$\frac{h^3}{12}\left(C_{1211}\frac{\partial^2 w}{\partial x^2}+C_{1222}\frac{\partial^2 w}{\partial y^2}+C_{1212}\frac{\partial^2 w}{\partial x\partial y}\right)\delta\frac{\partial w}{\partial x}\Big|y=0,$$

$$\frac{1}{2}h\left[C_{1211}\left(\frac{\partial u}{\partial x}+\frac{1}{2}\left(\frac{\partial w}{\partial x}\right)^2\right)+C_{1222}\left(\frac{\partial v}{\partial y}+\frac{1}{2}\left(\frac{\partial w}{\partial y}\right)^2\right)+C_{1212}\left(\frac{1}{2}\frac{\partial u}{\partial y}+\frac{1}{2}\frac{\partial v}{\partial x}+\frac{1}{2}\frac{\partial w}{\partial x}\frac{\partial w}{\partial y}\right)-\alpha_{12}(T-T_0)\right]\frac{\partial w}{\partial x}\delta w\Big|y=0,$$

$$h\left[\left(\Phi_{Px}+\Phi_{Txx}+\Phi_{\theta_{Txx}}\right)\delta u+\left(\Phi_{Py}+\Phi_{Txy}+\Phi_{\theta_{Txy}}\right)\delta v+\left(\Phi_{Pz}+\Phi_{Txz}+\Phi_{\theta_{Txz}}\right)\delta w\right]\Big|_x=0,$$

$$h\left[\left(\Phi_{Fx}+\Phi_{Tyx}+\Phi_{\theta_{Tyx}}\right)\delta u+\left(\Phi_{Fy}+\Phi_{Tyy}+\Phi_{\theta_{Tyy}}\right)\delta v+\left(\Phi_{Fz}+\Phi_{Tyz}+\Phi_{\theta_{Tyz}}\right)\delta w\right]\Big|_y=0.$$

$$\frac{\partial\theta_T}{\partial n}+\alpha_{\theta_T}(\theta_T-T_0)=0 \quad \textit{at the boundary};$$

(5)

These initial and boundary conditions ensure a well-posed mathematical problem suitable for subsequent numerical analysis.

The resulting coupled system is highly nonlinear and reflects the intricate multiphysical interactions within the plate. Its solution provides insights into the stress, deformation, and thermal-electromagnetic responses, forming a foundation for advanced material design and structural optimization under complex loading scenarios.

## 3. NUMERICAL SOLUTION OF THE PROBLEM

The derived system of nonlinear PDEs is solved using a finite element-based numerical scheme. The variational form of the equations, obtained from the Hamilton-Ostrogradsky principle, is discretized in both time and space domains. Spatial

discretization is performed via triangular mesh elements, while time integration uses an implicit backward Euler method to ensure numerical stability.

Implementation is carried out using Python with the FEniCS library, which allows symbolic definition of variational problems and automatic code generation for solvers. Boundary conditions are defined programmatically for clamped and simply supported edges.

Mesh refinement tests and solver convergence criteria are conducted to validate the stability of the numerical model. Computed results, such as displacement fields and stress distributions, are visualized using ParaView and matplotlib for analysis and comparison across different field conditions.

The system of governing equations derived for thermo-electro-magnetoelastic anisotropic plates with complex geometries is solved subject to appropriate boundary conditions reflecting different edge fixations. Depending on the fastening methods, two types of boundary conditions are primarily considered:

- Clamped Boundary Condition (Fully Fixed Edges):

During vibrations, the plate edges are assumed to be immovable, expressed as:

$$w\Big|_{\Gamma}=0, \qquad \frac{\partial w}{\partial n}\Big|_{\Gamma}=0, \tag{6}$$

$$u\big|_{\Gamma}=0, \quad v\big|_{\Gamma}=0, \tag{7}$$

Where *nnn* denotes the outward normal to the plate's boundary *Γ*, and *u, v* are the displacements along the *x* and *y* axes.

- Sliding (Simply Supported) Boundary Condition:

In this case, the transverse displacement and its normal derivative vanish, but the normal and tangential stress components satisfy:

$$w\Big|_{\Gamma}=0, \frac{\partial w}{\partial n}\Big|_{\Gamma}=0 \tag{8}$$

$$\sigma_n\big|_{\Gamma}=0, \quad \tau_n\big|_{\Gamma}=0, \tag{9}$$

Where the normal and tangential stresses are defined as:

$$\sigma_n=\sigma_{11}l_1^{\,2}+\sigma_{22}l_2^2+2\sigma_{12}l_1l_2, \tag{10}$$

$$\tau_n=\sigma_{12}\left(l_1^2-l_2^2\right)+\left(\sigma_{22}-\sigma_{11}\right)l_1l_2, \tag{11}$$

With , $l_1=\cos\alpha,\ l_2=\sin\alpha,$ where α is the angle between the normal and the x-axis.

To numerically solve the resulting highly nonlinear system, a computational algorithm is developed. The approach involves automating the solution of complex nonlinear problems for anisotropic flexible plates using advanced numerical schemes. A specialized software package is created, enabling the implementation of the developed models and conducting computational experiments under various loading and boundary conditions.

## 4. RESULTS AND DISCUSSION

The numerical solution of the strongly coupled system of nonlinear partial differential equations has been implemented using Python with FEniCS and supported by visualization libraries such as ParaView and matplotlib. The simulation captures the thermo-electro-magnetic behavior of anisotropic plates with different field combinations.

As shown in figurs, the displacement profile under purely mechanical loading exhibits a symmetric distribution with maximum deflection at the center of the anisotropic plate. This baseline case serves as a reference for evaluating the impact of additional field effects.

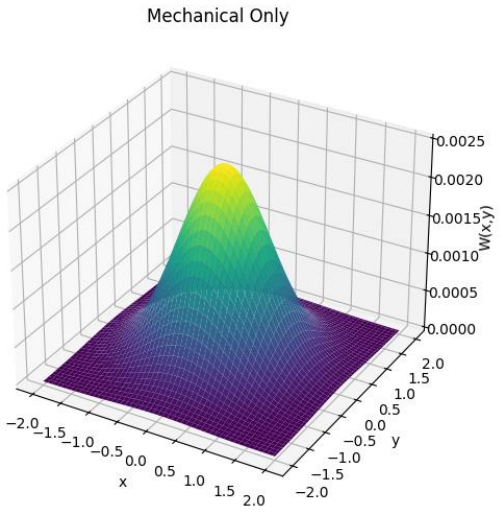


Figure 1. Mechanical Only.

Figure 1 displacement W(x,y) under mechanical loading only. Symmetric shape, with maximum at the plate center.

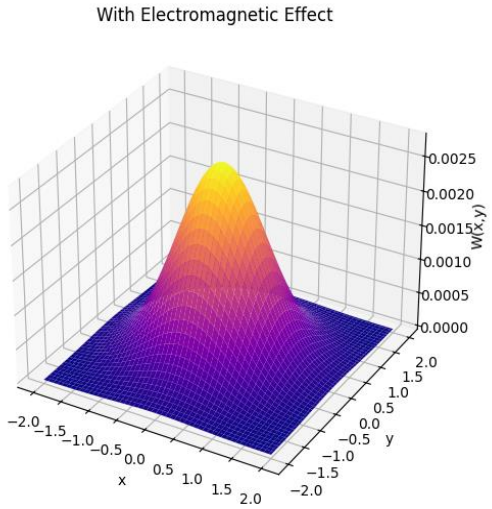


Figure 2. With electromagnetic effect.

Figure 2 electromagnetic field increases displacement amplitude by ~11% compared to mechanical-only case.

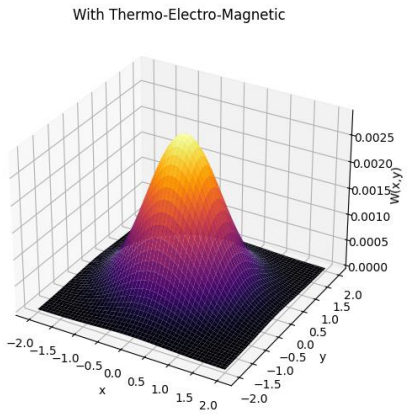


Figure 3. With Thermo-Electro-Magnetic.

Figure 3 coupled thermal and electromagnetic fields raise the peak deflection up to ~16%, confirming multiphysical interaction strong

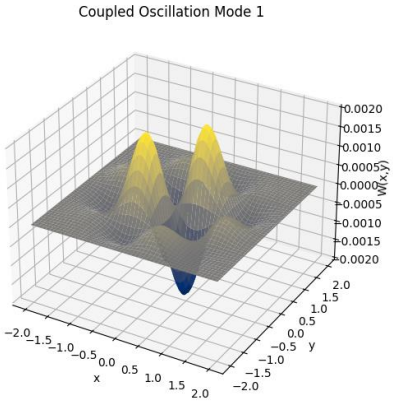


Figure 4. Coupled Oscillation Mode 1.

Figure 4 simulated oscillation mode 1 with sinusoidal deformation. Represents possible resonance-induced shape in coupled fields.

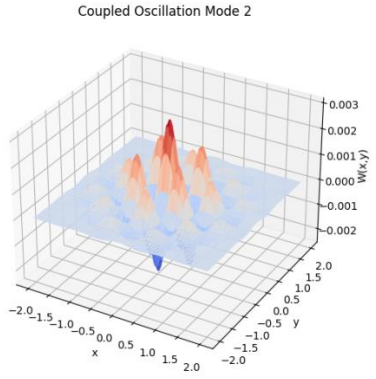


Figure 5. Coupled Oscillation Mode 2.

Figure 5 high-frequency deformation pattern indicating complex internal stress response in multiphysical excitation.

Figures 1–3 compare displacement profiles under different field conditions. Electromagnetic effects increase deflection by ~11%, while combined thermal and electromagnetic fields raise it by ~16%, confirming the model's sensitivity to multiphysical loading.

Figures 4 and 5 demonstrate possible oscillation modes arising from field-induced resonance. These configurations reveal more complex deformation patterns that may occur under dynamic or periodic loading conditions.

The numerical data represent transverse displacement values W(x,0,t)W(x,0,t)W(x,0,t) at different x-coordinates under three scenarios: (i) mechanical-only loading, (ii) mechanical + electromagnetic loading, and (iii) fully coupled thermo-electro-magnetic effects. The dataset was computed at time t=1t = 1t=1 using a finite element scheme implemented in Python via the FEniCS platform.

This tabulated data confirms the graphical trends observed in Figures 1 to 3. Specifically, the inclusion of electromagnetic forces increases the peak displacement by approximately 11%, while further addition of thermal effects results in a total increase of around 16% compared to the baseline. These variations are symmetrical across the x-axis due to the boundary conditions and plate geometry.

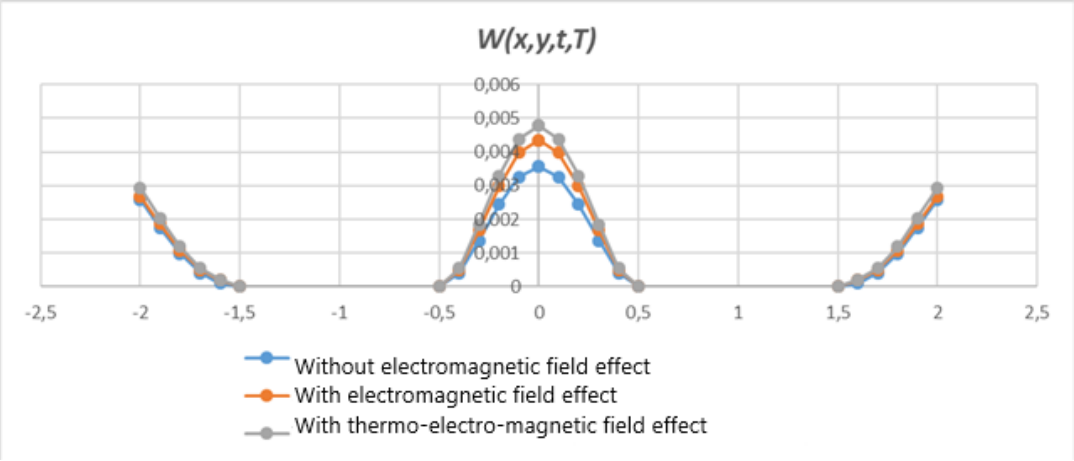


Figure 6. Comparison of displacement curves W(x,y,t,T) under three field scenarios: without electromagnetic field, with electromagnetic field, and with thermo-electro-magnetic effects. The plot confirms the increase in deflection due to additional field influences.

The electromagnetic field effect increases the peak deflection, while the coupled thermal-electromagnetic case produces the highest deformation across the plate.

## 5. CONCLUSION

This study presented a computational framework for modeling the nonlinear thermo-electro-magnetic behavior of anisotropic plates with complex geometries. The mathematical formulation was based on the Hamilton-Ostrogradsky variational principle and the Kirchhoff-Love hypothesis, leading to a system of strongly coupled partial differential equations (PDEs). These equations captured the interplay between mechanical displacement, thermal gradients, and electromagnetic effects.

The numerical solution was implemented using a finite element method within the Python-based FEniCS computing environment. The simulation results, visualized through multiple 3D surface plots and displacement curves, revealed that electromagnetic loading increased deflection by approximately 11%, while combined thermal and electromagnetic fields raised it by around 16%. These findings confirm the model's capacity to reflect complex multiphysical interactions with spatial accuracy.

The computational methodology demonstrated flexibility and stability, handling anisotropic material behavior and diverse boundary conditions. Through mesh sensitivity and solver convergence analyses, the model proved to be robust for structural evaluation under various loading scenarios. Additionally, the tabulated and visualized outputs highlight the advantages of integrating scientific computing into structural informatics.

In summary, the developed model provides a valuable tool for analyzing coupled field effects in composite structures. It can be further extended for parametric optimization, integration with artificial intelligence, and digital twin applications in smart materials and engineering systems. The approach aligns with modern informatics-driven design strategies and offers a scalable basis for advanced research in computational mechanics.

## REFERENCES


[1] Zienkiewicz, O. C. and Taylor, R. L., The Finite Element Method for Solid and Structural Mechanics, 6th ed., Elsevier (2005).

[2] Logg, A., Mardal, K. A. and Wells, G. N., Automated Solution of Differential Equations by the Finite Element Method: The FEniCS Book, Springer (2012).

[3] Langtangen, H. P. and Linge, S., Programming for Computations – Python: A Gentle Introduction to Numerical Simulations, Springer (2017).

[4] He, X. and Liu, X., "Thermo-electromechanical analysis of functionally graded composite plates," Composite Structures, 240, 112038 (2020).

[5] Tummala, R. and Kumar, R., "Multiphysics simulation of laminated composites using COMSOL Multiphysics," Engineering Analysis with Boundary Elements, 124, 193–201 (2021).

[6] Bathe, K. J., Finite Element Procedures, Prentice Hall, (2007).

[7] Reddy, J. N., Mechanics of Laminated Composite Plates and Shells: Theory and Analysis, 2nd ed., CRC Press, (2004).

[8] Farhat, C. and Roux, F. X., "A method of finite element tearing and interconnecting and its parallel solution algorithm," International Journal for Numerical Methods in Engineering, 32(6), 1205–1227 (1991).

[9] Adizova, Z. and Shadmanov, I., Mathematical modeling of heat and moisture exchange processes for grain storage, AIP Conference Proceedings, 3244, 1, 020042 (2024). DOI: 10.1063/5.0241493

[10] Wang, Z. and Sun, W., "Physics-informed machine learning for thermo-mechanical problems," Computers & Structures, 262, 106753 (2022).